ELSEVIER

Applied Catalysis A: General 162 (1997) 181–191

APPLIED CATALYSIS A: GENERAL

Synthesis of high surface area silicon carbide by fluidized bed chemical vapour deposition

R. Moene[1,a], L.F. Kramer[a], J. Schoonman[b], M. Makkee[a,*], J.A Moulijn[a]

[a]*Department of Chemical Engineering, Section Industrial Catalysis, Delft University of Technology, Julianalaan 136, 2628 BL Delft, Netherlands*

[b]*Department of Inorganic Chemistry and Thermodynamics, Section Applied Inorganic Chemistry, Delft University of Technology, Julianalaan 136, 2628 BL Delft, Netherlands*

Received 6 December 1996; received in revised form 28 February 1997; accepted 3 March 1997

Abstract

Activated carbon granulates loaded with small amounts of nickel have successfully been converted into high surface area silicon carbide granulates by reaction with hydrogen and silicon tetrachloride at 100 kPa and 1380 K ($C+SiCl_4+2H_2 \rightarrow SiC+4HCl$). A cone shaped Fluidized Bed Chemical Vapour Deposition reactor is demonstrated to achieve reproducible and homogeneous conversions of considerable amounts of activated carbon. High surface area silicon carbide has thus been synthesized with surface areas ranging between 25 and 80 $m^2 g^{-1}$. The shape memory concept is applicable, because the shape of the activated carbon determines the morphology of the silicon carbide. The conversion process is shown to be limited by the gasification of carbon into methane. The formed methane is then totally converted into SiC via the Vapour Liquid Solid mechanism and conventional Chemical Vapour Deposition. Carbon conversions range from 10% to 45%. The high surface area SiC obtained after conversion and removal of the residual carbon has high potential as catalyst support for liquid-phase application at demanding pH conditions and processes operating at high temperatures. © 1997 Elsevier Science B.V.

Keywords: Silicon carbide; Fluidized bed chemical vapor deposition; Vapor liquid solid mechanism; High surface area

1. Introduction

High surface area silicon carbide can have great potential as catalyst support for processes operating at high temperatures and demanding pH conditions owing to its inert surface, high thermostability and high thermal conductivity. Vannice et al. [1] synthesized SiC of nearly 50 m^2/g via gas-phase decomposition of $Si(CH_3)_4$ at temperatures of 1700 K. Shaping of the powder is, however, expected to be difficult and will probably result in a severe decrease in surface area. Ledoux et al. [2] synthesized SiC with a surface area of nearly 60 $m^2 g^{-1}$ by reacting SiO with activated carbon. The macro structure of the activated carbon is thus retained, which overcomes additional shaping of the SiC. The maximal conversion of carbon into SiC is 50% due to stoichio-

*Corresponding author. Tel.: +31 15 2781391; fax: +31 15 2784452; e-mail: m.makkee@stm.tudelft.nl

[1]Present address: Koninklijke/Shell-Laboratorium, Amsterdam, Badhuisweg 3, 1031 CM Amsterdam, Netherlands.

PII S0926-860X(97)00096-3

metric formation of carbon monoxide. Difficulties in conversion are to be expected due to slow diffusion of reactants through the product layer which is inherent for gas–solid reactions. Other methods of synthesis are mainly based on solid-state reactions like organic gel pyrolysis [3,4]. A novel catalytic method for converting activated carbon into high surface area SiC has recently been developed and described by Moene et al. [5,6]. The carbon is hereby gasified by hydrogen into methane, which subsequently reacts within the particle with silicon tetrachloride to form SiC. Both reactions are simultaneously catalyzed by nickel. The porous carbon acts thus as a reactant as well as template.

$$C(s) + 2H_2(g) \rightarrow CH_4(g) \quad (1)$$

$$SiCl_4(g) + CH_4(g) \rightarrow SiC(s) + 4HCl(g) \quad (2)$$

It has been shown that reaction (2) ensues partly via the Vapour Liquid Solid (VLS) mechanism resulting in high rates of SiC whisker formation. Synthesis of shaped SiC extrudates with surface areas of 30–57 $m^2 g^{-1}$ has shown to be feasible by conversion of activated carbon extrudates at 1380 K and 8 kPa in a fixed bed reactor. Typical carbon conversions range from 20% to 55%. The maximum amount of carbon to be converted in one batch was limited to about 0.2 g in this fixed bed configuration in order to achieve a sufficiently homogeneous conversion throughout the bed. Fluidized bed reactors are well-suited for large scale operation of gas–solid reactions because of the good mixing of the solid phase. Fluidized Bed Chemical Vapour Deposition (FBCVD) reactors have been used for this reason to coat particles with SiC [7–9] and Al and Ti [10]. In this paper the conversion of activated carbon granulates into high surface area SiC in a FBCVD reactor is reported. Larger amounts of activated carbon can thus homogeneously be converted enabling the characterization and testing of the high surface area SiC as catalyst support.

2. Experimental

2.1. Materials

The physical properties of the applied Norit activated carbons are given in Table 1. The Azo carbon is sieved to obtain particles in the range of 63–180 μm and used without further pretreatment. The Elorit granulates are pre-fluidized for 3 h to remove the fines and decrease the initial attrition of the carbon. A sieve fraction with a diameter of 300–425 μm has been selected for conversion. In some cases this fraction has previously been subjected to a washing procedure. This comprised subsequent washing with 5 l of a 0.5 M NaOH solution (duration 8 h), demineralized water until pH<8, 5 l of a 0.5 M HCl solution (duration 8 h), and, finally, demineralized water until pH>6. This washing procedure resulted in a decrease in ash content from 8 to 5 wt%. Nickel nitrate hexahydrate (>99%) and silicon tetrachloride (>98%), both from Janssen Chemica, were used. Activated carbon extrudates were loaded with nickel by pore volume impregnation of the carbon with a solution of $Ni(NO_3)_2 \cdot 6H_2O$ in demineralized water to arrive at nickel contents of 2, 5, or 8 wt% nickel. Drying was performed at atmospheric pressure in air at 385 K. The gases used for carbon conversion, argon and hydrogen, were purified by passing them over a Cu/Al_2O_3 or Pd/Al_2O_3 catalyst, respectively, followed by drying by molecular sieve 5A.

2.2. Conversion of activated carbon granulates

A schematic picture of the CVD apparatus is shown in Fig. 1. The carbon is fluidized in the cone-shaped quartz reactor (entrance diameter 2.7 mm, cone angle 7°, cone length 140 mm) surrounded by an alumina tube. The gas velocity at the cone entrance exceeds the rate of entrainment of the carbon, whereas the velocity in the upper part of the bed surpasses the minimal

Table 1
The physical properties of the activated carbon granulates

Carbon	S_{BET} ($m^2 g^{-1}$)	V_{pore} (ml g^{-1})	S_t ($m^2 g^{-1}$)	V_{micro} (ml g^{-1})	ρ(Hg) (kg m^{-3})	ρ(He) (kg m^{-3})	Ash (%)
Azo	703	0.88	219	0.23	690	2100	6.9
Elorit	655	0.6	149	0.25	600	2100	8

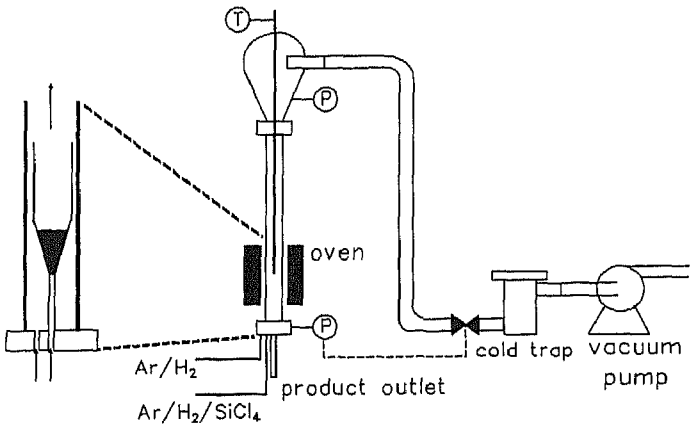

Fig. 1. Scheme of the fluidized bed CVD apparatus.

fluidization velocity. The pressure is regulated by a pressure transducer at the cone entrance and a butterfly valve in combination with a vacuum pump downstream of the system, which allows CVD experiments to be carried out at sub-atmospheric pressures. The reactor is loaded with activated carbon (typically 3–5 g) under flowing argon (16.7 ml s^{-1}). Subsequently the reactor is evacuated twice to 10 kPa to remove oxygen while the flow rate is simultaneously decreased in steps to 2.5 ml s^{-1} to prevent entrainment of the particles out of the reactor. The reactor is heated under flowing argon to 1380 K at 100 kPa during which the nickel nitrate decomposes and the formed nickel oxide is carbo-thermically reduced to metallic nickel. The argon flow is subsequently lowered and hydrogen and silicon tetrachloride were admitted at the proper flow rates; the total flow rate equalled 16.7 ml s^{-1} (STP) and the pressure was kept at 100 kPa.

2.3. Determination of fluidization characteristics

The minimum fluidization velocity of the sieved activated carbon granulates has been determined at ambient conditions in an all-glass fluidized bed reactor by measuring the pressure drop over the bed as a function of the gas (nitrogen) velocity and by visual confirmation of the bed behaviour. The fluidization regime under deposition conditions in the CVD reactor has been visually identified by replacing the alumina tube of the CVD reactor by a glass one. Pressure adjustment has been used to arrive at similar gas velocities as those under the high temperature CVD conditions.

2.4. Removal of residual carbon

The residual carbon, present after conversion, has been removed by oxidation in dry air at 1023 K in a tubular reactor.

2.5. X-ray diffraction (XRD)

X-ray diffractograms were measured with a Philips powder diffractometer (PW1840) using Cu K_α radiation (wavelength 0.154 nm).

2.6. Scanning electron microscopy (SEM)

A JEOL (JSM-35) scanning electron microscope has been used to determine the morphology of the deposited phases. An acceleration voltage of 20 keV has been applied; the samples have been sputtered with gold or platinum to suppress charging during SEM analysis.

2.7. Thermal gravimetric analysis (TGA)

TGA has been carried out on a Stanton Redcraft (STA-1500) thermobalance. 20 mg samples were oxidized in air using a temperature increase of 0.167 K s^{-1} from room temperature to 1273 K. The

weight change and concomitant heat flux were recorded simultaneously. Combination of the weight increase after conversion and the amount of carbon present in the converted granulate allows a silicon and carbon mass balance to be made.

2.8. Surface area measurements

Nitrogen isotherms at 77 K were recorded on a Carlo Erba Sorptomatic 1800. Prior to measurement the samples were degassed at 423 K and 0.1 kPa. The BET surface area (S_{BET}), t surface area (S_t) and micropore volume (V_{micro}) were determined according to Brunauer et al. [11] and de Boer et al. [12].

2.9. Particle size distribution

Measurements of particle size distributions have been performed on a Malvern 2600 particle sizer, using the principle of Fraunhofer diffraction.

3. Results

3.1. Fluidization characteristics

The particle size distributions after sieving of the Azo and Elorit activated carbon are characterized by d_{10}: 95 μm, d_{50}: 161 μm, and d_{90}: 261 μm and d_{10}: 324 μm, d_{50}: 456 μm, and d_{90}: 691 μm, respectively. These distributions appear to fall outside the range of diameters classified by sieving. This effect is, however, the consequence of a combination of non-sphericity of the carbon particles (the shape is a mixture of flake-like and cylinder-like) and the analysis method (the surface rather than the volume is analyzed). The minimum fluidization (u_{mf}) velocity of the Azo has been determined to be lower than 10 mm s^{-1}; the minimum bubbling velocity (u_{mb}) equalled 15 mm s^{-1}. Fluidization at reaction conditions in the CVD reactor demonstrated that the bed slugs severely, material loss occurs additionally through entrainment. The u_{mf} and u_{mb} of the Elorit have been determined to be 21 and 42 mm s^{-1}, respectively. The voidage (ϵ) of the bed in the CVD reactor as a function of the superficial gas velocity is shown in Fig. 2. No characteristic superficial gas velocity (u_0) can be defined due to the use of the cone shaped reactor. Hence, u_0 has been normalized to the start-up superficial gas velocity (u_i), viz. 16.7 ml s^{-1} argon at ambient conditions. The voidage of the bed at minimum fluidization velocity (u_o/u_i=0.7) is slightly higher than that of the packed bed voidage, viz. 0.62. Above u_o/u_i=1.8 slugging starts, the bed expands considerably; the total void fraction approaches 0.95 at high gas velocities.

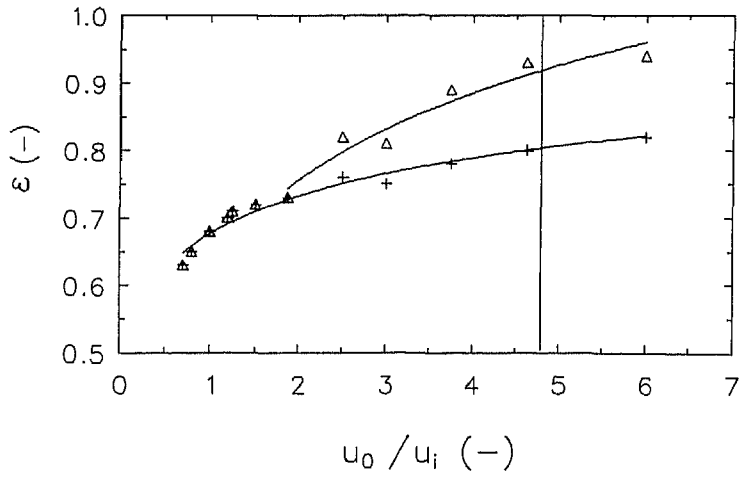

Fig. 2. Voidage (ϵ) vs. superficial gas velocity for the observed bed height (+) and maximum slug height (△) (Elorit carbon). Conversion at u_0/u_i=4.8.

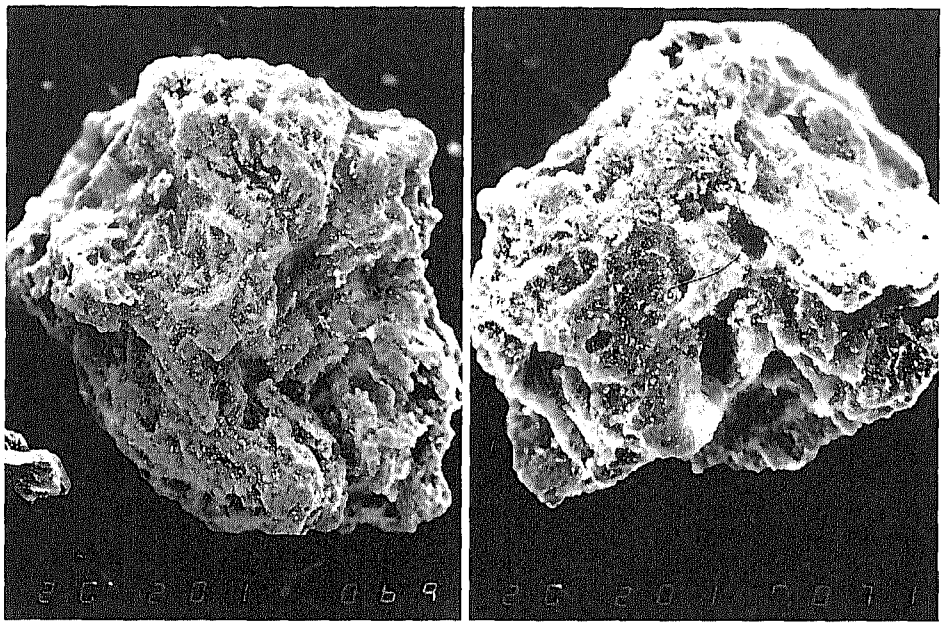

Fig. 3. The shape memory concept. The left-hand panel is a micrograph of a granulate after conversion into SiC; the right-hand panel is a micrograph of another granulate after oxidation. (———) 100 μm

3.2. Morphology of the converted granulates

Crystalline silicon carbide is detected by XRD after conversion of the Azo and Elorit at 1380 K in all cases. No crystalline silicon has been detected. Conversion of Elorit at lower temperatures (1330 K) resulted in silicon co-deposition. Removal of the residual carbon reveals that the shape memory concept is valid for this conversion process; no differences in particle diameter are encountered comparing the original and converted–oxidized carbon; Fig. 3 displays an example. SEM analysis of the SiC morphology discloses the presence of SiC whiskers grown via the Vapour Liquid Solid (VLS) mechanism [5,6].

3.3. Rates of methane and silicon carbide formation

The rates of methane and silicon carbide formation can be determined independently by using a carbon and silicon mass balance. Both are obtained from TGA data which measure the amount of carbon and non-oxidizable material by combustion in air.

3.4. Azo activated carbon with 5 wt% nickel

Due to the rate of entrainment of the Azo carbon resulting in carbon loss during conversion, no reliable carbon and silicon mass balances could be obtained. Evaluation of the amount of silicon carbide present in the carbon after conversion can, however, be used as a first indication for the conversion characteristics in the FBCVD reactor. The results are displayed in Fig. 4. A linear relationship between the H_2 content and amount SiC formed can be deduced, although the confidence region is quite large. The influence of $SiCl_4$ partial pressure on the amount of SiC formation is not significant.

3.5. Elorit activated carbon

The rate of gasification without SiC formation has been determined by reacting 5 wt% Ni/Elorit with a H_2/Ar mixture ($X_{H_2} = 0.45$) at 1380 K for 40 min. The total carbon conversion equalled 5.5%. The carbon and silicon mass balance for the converted Elorit activated carbon can be determined, because significant entrainment does not occur and the pre-fluidiza-

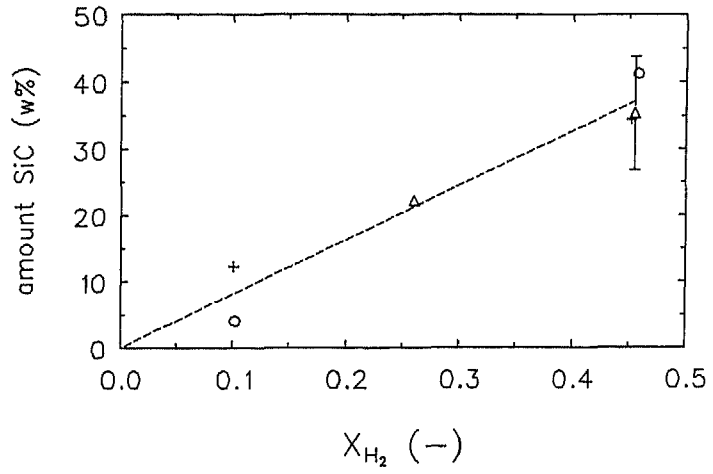

Fig. 4. SiC in Azo activated carbon after conversion vs. the molar fraction of H_2 in the feed for X_{SiCl_4}: (+) 0.045%, (△) 0.090%, (○) 0.13%. The 95% confidence region (two experiments) is included.

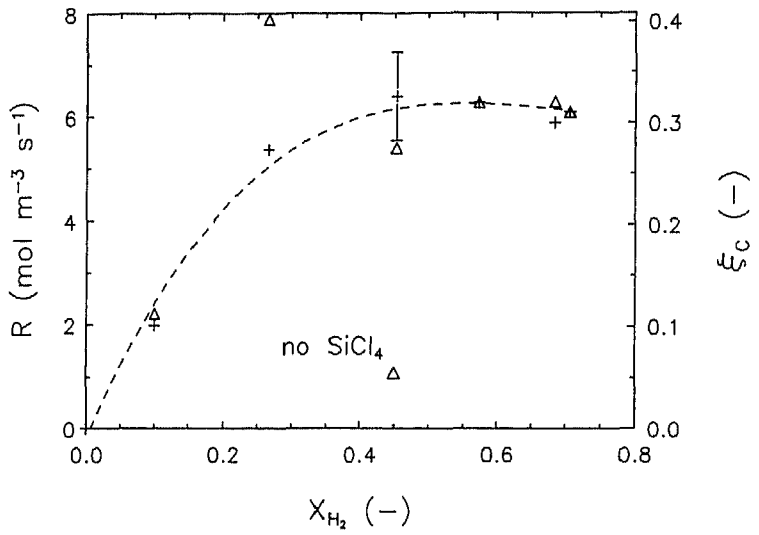

Fig. 5. Rate of CH_4 (△) and SiC (+) formation and corresponding carbon (Elorit) conversion at 1380 K vs. hydrogen content for 5 wt% Ni/Elorit, reaction time: 40 min.

tion lessened the attrition during conversion substantially.

Some attrition and subsequent material loss through entrainment still transpires, however, which impose a modest error in the calculation of the rate of gasification and the rate of SiC formation. The results of the conversion are given in Fig. 5, which displays the rate of CH_4 and SiC formation and related carbon conversions for Elorit carbon loaded with 5 wt% nickel.

Carbon conversions vary between 0.1 and 0.3 for the conditions investigated. The conversion achieved in the absence of $SiCl_4$ (0.055) is considerably lower than that in the presence of SiC formation (0.3). The 95% confidence region has been determined from two

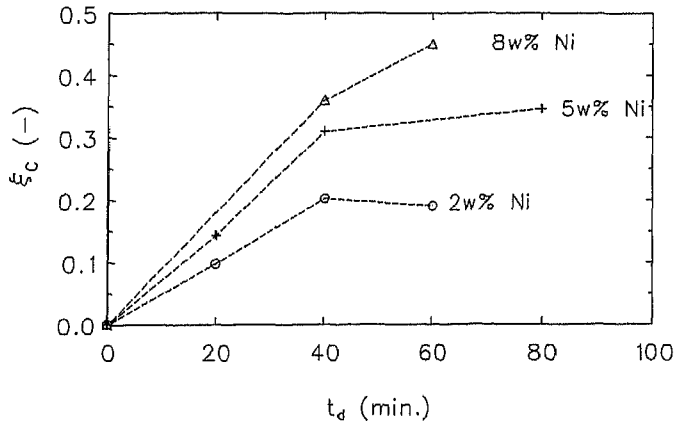

Fig. 6. Carbon (Elorit) conversion vs. reaction time at 1380 K. 2 wt% Ni: $X_{H_2} = 0.27$, $X_{SiCl_4} = 0.046$ (○); 5 and 8 wt% Ni: $X_{H_2} = 0.45$, $X_{SiCl_4} = 0.046$, (+) and (△), respectively.

experiments conducted at identical conditions. The amount of SiC present in these converted granulates is 50.6 and 48.6 wt%, respectively. This corresponds to carbon conversions of 0.32 and 0.305, demonstrating that the product composition is virtually identical, and that the large 95% confidence region is mainly imposed by the small number of experiments.

An almost linear correlation appears to exist between the reaction rate and H_2 content below 45 mol%. No increase in carbon conversion is found for H_2 concentration above 45 mol% indicating that the maximum conversion has been reached. The carbon conversions for various nickel loadings are shown as a function of reaction time in Fig. 6. It should be noted that the mole fraction hydrogen used in the experiments with 2 wt% Ni/Elorit is 0.27 instead of 0.45 as for the other experiments. The carbon conversion increases in the initial stage (up to 40 min) linearly with the reaction time, after which the conversion stopped. Higher nickel loadings result in higher final conversions and higher rates of conversion. Conversion of 5 wt% Ni/Elorit at a sub-atmospheric pressure of 50 kPa ($X_{H_2} = 0.46$, $X_{SiCl_4} = 0.045$, 40 min) resulted in a SiC content in the carbon of 39 wt% and a corresponding carbon conversion of 0.19.

Elorit subjected to a washing procedure displayed a carbon conversion which was slightly lower than that of the unwashed carbon. Fourteen batches of high surface area SiC have been prepared at the following conditions (1380 K, 100 kPa, X_{H_2}: 0.45, X_{SiCl_4}: 0.045, t: 40 min). The average carbon conversion was 0.2614±0.0087. The small 95% confidence region evidences the highly reproducible performance of the experimental set-up.

3.6. Texture of high surface area SiC

The results of surface area analyses of the converted Elorit granulates are shown in Table 2. The BET

Table 2
Surface area (BET and t) of high surface area SiC, the conditions of conversion correspond to those of Fig. 6 at 40 min conversion

	2 wt% Ni		5 wt% Ni		5 wt% Ni[a]		8 wt% Ni	
	S_{BET}	S_t	S_{BET}	S_t	S_{BET}	S_t	S_{BET}	S_t
After conversion	300	87	154	n.d.	206	66	137	49
After oxidation	80	66	25	n.d.	31	23	34	30

n.d. – not determined.
[a]Washed carbon.

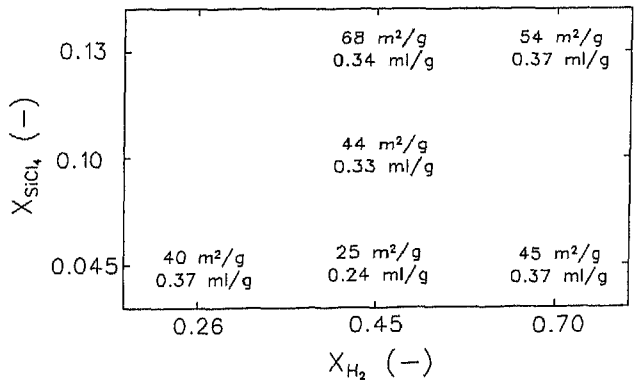

Fig. 7. BET surface areas and pore volume for converted and oxidized 5 wt% Ni/Elorit (not washed) as a function of gas composition, reaction time: 40 min.

surface area comprises both the micro- and meso-pore areas, whereas the t surface area contains only the surface area of the meso pores. The surface area after conversion ranges from 137 to 300 $m^2 g^{-1}$ and is composed of the original carbon and the SiC, shown by the substantial amount of micro-pore surface. The SiC surface ranges from 31 to 80 $m^2 g^{-1}$ and contains primarily meso pores.

The influence of gas composition (H_2 and $SiCl_4$ content) on the texture after conversion and oxidation is displayed in Fig. 7. The surface areas extend between 25 and 68 $m^2 g^{-1}$, while the pore volumes range from 0.24 to 0.37 $m^3 g^{-1}$. The results indicate that the highest surface areas are obtained at the highest $SiCl_4/H_2$ ratios. The influence of H_2 on the textural properties is not clear. The washing procedure significantly affects the texture by elevating the residual surface area from 25 (Fig. 7) to 31 $m^2 g^{-1}$ (Table 2).

The influence of conversion time on the texture is demonstrated in Table 3. The surface area and pore volume remain virtually constant up to 40 min of conversion, whereas a significant enlargement is achieved in the final stage.

Table 3
The texture of converted 5 wt% Ni/Elorit ($X_{H_2} = 0.45$, $X_{SiCl_4} = 0.045$) after oxidation as a function of conversion time

	Conversion time		
	20 min	40 min	80 min
S_{BET} ($m^2 g^{-1}$)	28	25	42
V_{pore} (ml g^{-1})	0.22	0.24	0.29

3.7. Influence of pressure

Table 4 displays the results of sub-atmospheric conversion compared to atmospherically conducted experiments. Although the H_2 concentration is not identical for the two experiments, it can tentatively be concluded that performing the reaction at sub-atmospheric pressures lowers the rate of conversion.

4. Discussion

4.1. Fluidization characteristics

The FBCVD reactor operates for both the Azo and Elorit carbon in the slugging mode during conversion.

Table 4
Influence of pressure on the conversion of carbon (5 wt% Ni Elorit, $X_{SiCl_4} = 0.045$)

Experiment	P (kPa)	F^{STP} (ml min^{-1})	X_{H_2}	C_{H_2} (mol m^{-3})	t (min)	Amount SiC (wt%)	ξ_C
1	50	500	0.46	2.0	40	35	0.19
2	100	1000	0.27	2.2	40	48	0.26

This causes considerable particle loss in the low diameter range, especially for the Azo. Major entrainment of the larger Elorit particles does not occur owing to the pretreatment procedure of the Elorit. The major contribution to particle loss, i.e. attrition, has been reduced sufficiently to obtain reasonable accurate mass balances.

According to the Geldart classification [13], for particles in fluidized bed technology, Elorit is located on the edge of the 'A' and 'B' regions. An important distinction between these two is that only Geldart A particles differ in minimal fluidization velocity (u_{mf}) and minimal bubbling velocity (u_{mb}), whereas in beds of Geldart B particles bubbles form as soon as the gas velocity exceeds u_{mf}. Elorit can be classified as a Geldart A particle because bubbling starts at $2u_{mf}$. Other characteristics of Geldart A particles are that gas bubbles rise more rapidly than the rest of the gas, which percolates through the emulsion. These bubbles appear to split and coalesce frequently as they rise through the bed. Cross circulation of solids occurs even when only a few bubbles are present. This circulation is especially pronounced in large beds [13]. At the onset of fluidization the voidage of the bed should equal that of a packed bed, which in fact was experimentally found.

Another important parameter in fluidization technology is the sphericity factor (ϕ_s), which is used to correct for the non-sphericity of the particles and defined by

$$\phi_s = \left(\frac{S_{sphere}}{S_{particle}}\right)_{constant\ V}. \quad (3)$$

Reasonable values for Elorit should lie between 0.44 and 0.63 according to Kunii and Levenspiel [13]. An estimation of ϕ_s can be acquired from Eq. (4), which is generally used to predict the u_{mf} from known particle properties.

$$\frac{1.75}{\epsilon_{mf}^3\phi_s}\left(\frac{d_p u_{mf}\rho_g}{\mu}\right)^2 + \frac{150(1-\epsilon_{mf})}{\epsilon_{mf}^3\phi_s^2}\left(\frac{d_p u_{mf}\rho_g}{\mu}\right) = \frac{d_p^3\rho_g(\rho_s-\rho_g)g}{\mu^2}, \quad (4)$$

which simplifies for small particles and $Re_{p,mf}<20$ to

$$u_{mf} = \frac{d_p^2(\rho_s-\rho_g)g\epsilon_{mf}^3\phi_s^2}{150\mu(1-\epsilon_{mf})}. \quad (5)$$

Calculation of ϕ_s using Eq. (5), the experimentally determined u_{mf} and ϵ_{mf}, and a mean particle diameter of 456 μm results in a value of ϕ_s below 0.3, which is well outside the range expected. No ideal behaviour is, however, to be expected because the size distribution of particles is quite wide. The smaller particles are able to slip into the void spaces between the larger particles, and fluidize while the larger ones remain stationary. Using the d_{10} as characteristic particle size following Schouten [14] the sphericity factor equals 0.38, which show that the granulate shape deviates considerably from spherical particles.

4.2. Conversion characteristics

Conversion of activated carbon granulates into SiC in the FBCVD reactor is shown to be feasible; carbon conversions up to 45% have been achieved. Moreover, the liberty of utilization of atmospheric pressure facilitates the operation to a large extent compared to fixed bed experiments [5,6].

4.3. Rate-determining step

Both the Azo and Elorit display a linear dependence between the H_2 (up to $X_{H_2} = 0.45$) content and the carbon conversion as was shown in Figs. 4 and 5. No relationship between the $SiCl_4$ content and the carbon conversion has been encountered. From these observations it can be deduced that the first reaction (hydrogasification, Fig. 1) is rate determining in the conversion. This is evidenced by the nearly 100% utilization of the formed CH_4 for SiC deposition. Additional confirmation is found in the very low SiC deposition on the reactor wall indicating that the conversion transpires totally inside the granulates. Each particle can thus be envisaged as a small batch reactor, providing itself with the necessary methane. Conversion of activated carbon extrudates displayed major internal diffusion limitations for $SiCl_4$ resulting in lower utilization of the formed CH_4 and SiC deposition downstream of the fixed bed [5]. Determination of the presence of internal diffusion limitations by calculation of the Wheeler–Weizs number [14] for Elorit, however, shows the absence of diffusion limitations for both $SiCl_4$ and H_2 in the meso and macro pores allowing the conversion to proceed homogeneously

throughout the particles and to obtain a 100% CH_4 utilization. Moreover, in contrast to the extrudate conversions, no silicon is co-deposited during the synthesis of high surface area silicon carbide granulates. It was previously shown that Si co-deposits as a silicon rich SiC phase during SiC growth inflicted by a deficiency of methane in the region of the extrudate which had already partially been converted into SiC, see [5]. The homogeneous granulate conversion, however, provides a sufficiently high quantity of methane throughout the particle suppressing the local co-deposition of Si. The conversion halts abruptly and uniformly when the nickel which catalyzes the gasification is deactivated due to the formation of a silicide or due to reaction with the ash in the activated carbon, thus preventing silicon co-deposition.

The rate of gasification without SiC formation is substantially lower than that with SiC formation, which is quite remarkable because the presence of $SiCl_4$ is expected to deactivate a substantial amount of the gasification sites by forming whiskers or a nickel silicide granule during reaction. The formation of chlorine containing hydrocarbons as a gasification product cannot rationalize the higher rate of gasification, because thermodynamic calculations (unpublished results) have shown that the equilibrium concentrations of these products are several orders of magnitude lower than those of CH_4 and C_2H_4. The presence of hydrogen chloride in the pores may account for this effect by increasing the nickel dispersion causing higher rates of gasification. It is, however, imaginable as well that the thermodynamic limitation of Eq. (1)[5] determines the low amount of gasified carbon in the absence of SiC formation. The presence of $SiCl_4$ probably impedes the establishment of the thermodynamic equilibrium of Eq. (1) by removing the formed CH_4 via deposition of SiC. The fact that the concentration of $SiCl_4$ does not influence the rate of conversion should then be imposed by the achievement of maximum attainable rate of gasification at these conditions.

4.4. Influence of pressure

Table 4 displays the result of sub-atmospheric conversion compared to atmospherically conducted experiments. Experiment 2 is carried out using a similar W_C/F_{H_2} ratio and hydrogen concentration as the one in experiment 1 and results in a higher carbon conversion. Although the mole fraction H_2 is not identical for the two experiments, it can tentatively be concluded that performing the reaction at sub-atmospheric pressures lowers the rate of conversion. This can be ascribed to the pressure dependence of the thermodynamic equilibrium composition of Eq. (1). Decreasing pressures impose a lower equilibrium concentration of methane, which is expected to lower the rate of conversion.

4.5. Influence of washing

The washing procedure decreases the ash content of the activated carbon from 8 to 5 wt%, which improves the purity of the high surface area SiC. Washing decreases the carbon conversion and elevates the residual surface area of the SiC. The first effect might suggest that reaction of nickel with the ash during conversion is not the major cause of deactivation. The exact influence of the washing procedure on the conversion is, however, not completely clear.

4.6. Texture of high surface area SiC granulates

The shape memory concept holds for this conversion process, similar to that of the conversion of activated carbon extrudates [4]. After conversion the BET surface areas decrease from 655 to 300, 206, and 137 $m^2\ g^{-1}$, respectively for the 2, 5, and 8 wt% nickel loaded Elorit. Part of the decrease is caused by the weight increase by Si-deposition. The surface areas are corrected for deposition by normalization to the same volume as the original carbon (1 g Elorit). The results are displayed in Table 5. It can be concluded that the absolute surface areas decrease to a similar degree during conversion. The micro-pore surface area decreases to the largest extent caused by pore-mouth plugging during SiC deposition. The surface

Table 5
Surface area ($m^2\ g^{-1}_{carbon}$) of high surface area SiC

	2 wt% Ni		5 wt% Ni[a]		8 wt% Ni	
	S_{BET}'	S_t'	S_{BET}'	S_t'	S_{BET}'	S_t'
After conversion	395	115	351	112	235	91

[a]Washed carbon.

areas after oxidation (Table 2 and Fig. 7) suffice for application as catalyst support. Processes operating at high temperatures in which diffusion limitations are encountered provide future areas of utilization owing to the absence of micro pores.

5. Conclusion

A Fluidized Bed Chemical Vapour Deposition reactor is very well suited for the catalytic conversion of nickel loaded activated carbon into high surface area silicon carbide at 1380 K and pressures ranging from 50 to 100 kPa. The conversion process can be divided into a gasification step ($C+2H_2 \rightarrow CH_4$) and a CVD step ($SiCl_4+CH_4 \rightarrow SiC+4HCl$). It is shown that the first one is rate limiting in the conversion. Carbon conversions up to 45% have been achieved. No internal diffusion limitations are encountered during conversion. The surface area after conversion ranged from 137 to 300 $m^2\ g^{-1}$; removal of the residual carbon resulted in meso/macro porous SiC granulates with surface areas between 25 and 80 $m^2\ g^{-1}$. The properties of this high surface area SiC allow the use as catalyst support in processes working at elevated temperatures and liquid-phase processes operating at demanding pH conditions.

6. Nomenclature

d	diameter (m)
S	surface area (m^2)
S_{BET}	BET surface area ($m^2\ g^{-1}$)
S_t	t surface area ($m^2\ g^{-1}$)
t_d	conversion time
u_0	superficial gas velocity at STP ($m\ s^{-1}$)
u_i	superficial gas velocity ($m\ s^{-1}$)
u_{mb}	minimal bubbling velocity ($m\ s^{-1}$)
u_{mf}	minimal fluidization velocity ($m\ s^{-1}$)
V	volume (m^3)
V_{micro}	micro-pore volume ($ml\ g^{-1}$)
V_{pore}	pore volume ($ml\ g^{-1}$)
X	mole fraction

Greek symbols

ϵ	porosity (m^3 free space m^{-3})
ϕ_s	sphericity factor
μ	viscosity (Pa s)
ρ	density ($kg\ m^{-3}$)

Dimensionless number

Re	Reynolds

Acknowledgements

This research was part of the Innovation-oriented Research Programme on Catalysis (project number 90017) and was financially supported by the Ministry of Economic Affairs of The Netherlands.

References

[1] M.A. Vannice, C. Yu-Lin, R.M. Friedman, Appl. Catal. 20 (1986) 91.
[2] M.J. Ledoux, S. Hantzer, C. Pham Huu, J. Guille, M.-P. Desaneaux, J. Catal. 114 (1988) 176.
[3] P.W. Lednor, R. de Ruiter, in: J.E. Sheets (Ed.), Inorganic and Metal-Containing Polymeric Materials, Plenum Press, New York, 1990, p. 187.
[4] P.W. Lednor, Catal. Today 15 (1992) 243.
[5] R. Moene, L.F. Kramer, J. Schoonman, M. Makkee, J.A. Moulijn, Scientific bases for the preparation of heterogeneous catalysts, Sixth International Symposium, Louvain-la-Neuve, Preprints, vol. I, 1994, p. 379.
[6] R. Moene, M. Makkee, J.A. Moulijn, Catal. Lett. 34 (1995) 285.
[7] J.I. Federer, Thin Solid Films 40 (1970) 89.
[8] K. Minato, K. Fukuda, J. Nucl. Mater. 149 (1987) 233.
[9] S. Morooka, A. Kobata, K. Kusakabe, AIChE Sym. Ser. 87 (281) (1991), 32.
[10] B.J. Wood, A. Sanjurjo, G.T. Tong, S.E. Swider, Surf. Coat. Technol. 49 (1991) 228.
[11] S. Brunauer, P.H. Emmett, E. Teller, J. Amer. Chem. Soc. 60 (1938) 309.
[12] J.H. de Boer, B.G. Linsen, Th.J. Osinga, J. Catal. 4 (1965) 643.
[13] D. Kunii, O. Levenspiel, Fluidization Engineering, 2nd ed., Ellis Horwood, Chichester, UK, 1991.
[14] J.A. Moulijn, A. Tarfaoui, F. Kaptein, Catal. Today 11 (1991) 1.